Anomalous current transients related to defect discharge in irradiated silicon diodes

David Menichelli,* Monica Scaringella, and Mara Bruzzi
Department of Energetics, via S. Marta 3, 50139 Florence, Italy

Ioana Pintilie
National Institute of Materials Physics, 76900 Bucuresti-Magurele, Romania

Eckhart Fretwurst
Institute for Experimental Physics, Hamburg University, D-22761, Germany
(Received 25 March 2004; revised manuscript received 10 August 2004; published 15 November 2004)

Nonmonotonic current transients at constant temperature, following a pulsed charge injection, have been observed in silicon diodes heavily irradiated with gamma rays. The features of the transients have been studied at different temperatures and using various reverse biases. The particular shape of the measured transients is interpreted, with the help of numeric simulations, in terms of a strong time dependency of the space charge density due to the discharge of radiation induced deep traps. In particular, a nonmonotonic transient is generated if the discharge of a dominant trap determines the change of the space charge sign (type inversion). In this case the active volume of the sample, from which the current is collected, is increased during the discharge and causes the sample to become fully depleted for a short time. During this time interval the active volume reaches its maximum value and a peak is produced in the transient shape. The measurement of this peak provides a sensitive way to detect type inversion in semiconductor devices and to determine the responsible energy levels. The correlation of nonmonotonic transients with thermally stimulated current spectra and the distortion produced in deep level transient spectroscopy spectra are discussed in detail.

DOI: 10.1103/PhysRevB.70.195209 PACS number(s): 71.55.Cn, 72.20.Jv, 61.82.Fk, 29.40.Wk

I. INTRODUCTION

The study of defects in semiconductors is of fundamental relevance in solid-state physics and device technology. Defects and impurities introduce localized energy states within the band gap[1] and can severely influence the electrical properties of materials. The effect of deep levels on the semiconductor devices performance is of primary interest for the development of position-sensitive particle detectors in high energy physics experiments.[2,3] This applies to experiments at the future Large Hadron Collider (LHC) at CERN and at its possible upgrade SuperLHC[4] where hadron fluences up to 10^{16} cm^{-2} are foreseen. The standard silicon tracking detectors are $p^+/n/n^+$ devices produced from n-type float zone (STFZ) Si with resistivity of the order of 1 kΩ cm. Diffusion oxygenated float zone (DOFZ) silicon is used in some tracking areas too.[5] For the high fluence levels mentioned above, deep acceptor traps induced by radiation strongly influence the "effective doping concentration" $N_{\mathrm{eff}}=|Q/q|$, Q being the space charge density and q the elementary charge. Irradiation can eventually produce the sign change of Q. This phenomenon, known as type inversion of the space charge region, or space charge sign inversion (SCSI), is commonly observed in irradiated STFZ silicon. In the case of gamma irradiation from ^{60}Co, type inversion occurs after doses of 215 Mrad or higher.[6]

In samples with electrically active defects N_{eff} is determined by the occupancy of deep levels, which in turn depends on sample history (as carrier injection before measurement) and operational temperature. Its steady state value is usually measured by capacitance–voltage profiles at room temperature, and only few experiments to detect its variations with temperature have been carried out in the recent past.[7] The sign of Q can change due to the emission of carriers from a charged deep level dominating the space charge density. Abrupt modifications of Q and N_{eff}, including SCSI, after filling of the traps with nonequilibrium carriers at low temperature, have been recently related[8] to the observation of discontinuities in thermally stimulated currents[9] (TSC) spectra.

Capacitance and current transients at constant temperature, measured across a junction after a priming pulse, have been widely studied in the past.[10] This is because these techniques are suitable to study directly deep levels, and because they are the foundation of deep level transient spectroscopy (DLTS),[11] a powerful technique to study electrically active defects in semiconductors. The analysis of capacitance transients allows one to distinguish between majority and minority-carrier traps, whereas current transients are of special interest to study high resistivity and heavily defective materials.[12,13] Standard DLTS analysis applies when transients are exponential functions of time. Nonexponential transients can occur if the deep level emission coefficient exhibits a dependence on the electric field, or if the trap concentration N_t is not negligible in comparison to N_{eff}. Nonexponential transients have been studied by Wang and Sah[14] and by Phillips and Lowney.[15] However, the transients considered in all these works were monotonic, even if nonexponential. To our knowledge, nonmonotonic transients, showing a pronounced peak, have been observed only by Rosencher *et al.*[16] in silicon junction at cryogenic temperatures. This phenomenon was accounted for in terms of electric field assisted emissions, such as Poole-Frenkel barrier lowering and trapped carriers tunneling, leading identical traps in different places of the depleted region to emit with different rates.

In this paper we report the observation of nonmonotonic current transients in silicon diodes heavily irradiated with gamma rays, in the temperature range 100–250 K. This effect is interpreted in terms of charge emission from a few dominating traps, producing type inversion of the space charge region. The discussion is supported by the results of numerical simulations and TSC measurements.

II. EXPERIMENTAL PROCEDURES

A. Samples

The samples considered in this work are $p^+/n/n^+$ silicon diodes produced with different starting materials. Twin samples have been produced by CiS, Institute for Microsensors, Erfurt, Germany, from standard (STFZ) and oxygen diffused float zone (DOFZ) *n*-type Si with an initial resistivity of about 5 kΩ cm. The crystal orientation is $\langle 111 \rangle$ and the thickness is $w=285$ μm. The electrode active area on the p^+ side is $A_p=25$ mm^2, while the electrode on the n^+ side has an area $A_n=1$ cm^2. The oxygen diffusion technology, developed at Brookhaven National Laboratory,[17] has been systematically applied by the CERN RD48 and RD50 Collaborations[18] to increase the radiation hardness of Si particle detectors. In our DOFZ sample the oxygenation was performed for 72 h at 1150 °C. The samples have been irradiated at Brookhaven National Laboratory with gamma rays from a ^{60}Co source, up to a dose of 300 Mrad. After irradiation the STFZ sample showed type inversion at room temperature, with a change of N_{eff} from a donor concentration $N_{\text{eff}}=1.2\times10^{12}$ cm^{-3} before irradiation to an acceptor concentration $N_{\text{eff}}=6.0\times10^{10}$ cm^{-3}. In contrast, the DOFZ Si sample is not inverted by irradiation, showing a slight increase of donor concentration from $N_{\text{eff}}=8.3\times10^{11}$ cm^{-3} before irradiation to $N_{\text{eff}}=9.0\times10^{11}$ cm^{-3} after irradiation. The samples have been stored 6 months at room temperature before carrying out the measurements reported in this work, unless indicated differently in the text.

B. Experimental setup

The DLTS experimental setup, which is also used to sample current transients at constant temperature, is described in Fig. 1. The reverse bias V_{rev} and the forward voltage pulses V_{p} for sample excitation are provided by a pulse generator (Systron Donner 110D). The duration t_{p} of the excitation pulses can be varied starting from 1 μs. The current transients $i(t,T)$ are measured using a custom readout circuit. It converts the current into voltage, ensuring adequate values of transresistance $[r=(0.5-1)\times10^6$ V/A], input resistance ($R_{\text{in}}=2.2$ kΩ), and bandwidth (BWD=1 MHz). The readout circuit is a three stage amplifier. The first stage is a current–voltage converter, while the next two are voltage amplifiers. The same operational amplifier (Analog OP467G) was used to construct each stage. This device ensures fast recovering from saturation and the readout circuit can be used to clamp the forward current peak, which is superimposed on the deep levels emission. As a matter of fact, the forward current is much more intense than the deep levels signal, and it is necessary to permit the saturation of the amplifier during the excitation in order to detect the emission from traps. The whole readout circuit recovers its linear behavior from deep saturation in about 3 μs. The readout circuit output is monitored by a 500 MHz digital oscilloscope (Tektronix TDS520D) which samples the current transients. The test diode is located inside a vacuum chamber where a pressure lower than 10^{-3} mbar is maintained and which is cooled by a cryogenerator (Officine Galileo K1). The system is kept under vacuum to prevent the condensation of air humidity. The heating is provided by a resistor wounded around the sample support, and the heater power supply is controlled by the computer. Thus heating and cooling cycles with fixed rate can be obtained. In DLTS experiments we always adopted a heating rate slower than 0.07 K/s, in order to prevent spectrum distortion due to a fast temperature variation. During each current transient $i(t,T)$ acquisition the temperature was kept constant.

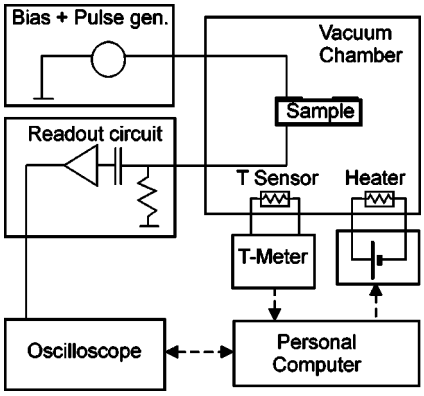

FIG. 1. Schematics of the setup used to measure current transient at constant temperature and DLTS spectra. Solid lines: analog electrical connections. Dashed lines: digital data flow.

A different setup is used for TSC measurements. In this case, the sample is cooled at the excitation temperature T_{p} by immersion in liquid helium vapor. T_{P} is determined by the sample holder height above the liquid He surface. A heating resistance allocated inside the sample holder increases the sample temperature. Reverse biasing and current reading are provided by a Keithley 617 electrometer. During excitation a forward bias is applied to the diode, in order to saturate the forward current at 3.8 mA. The filling time was always $t_f=1$ min. The system used to monitor the temperature is the same in the TSC and DLTS setups. The sensor is a silicon diode (Lake Shore DT-470-CU11) measured by a temperature controller (Lake Shore DRC91C). The temperature range investigated in this work is 100–250 K.

III. MODELING OF NONMONOTONIC CURRENT TRANSIENTS

For the modeling we consider an ideal $p^+/n/n^+$ diode. The electrode area A_n and A_p are different, as in the case of the test diodes used in our experiments. After high levels of irradiation the initial doping concentration, determined by phosphorus doping, is changed by the electrical active defects generated in the bulk. As an example, the deep trap for holes produced by the carbon-oxygen complex $C_iO_i^{+/0}$ is

considered.[19] We will assume this defect to be uniformly distributed in the silicon bulk. The signature of the corresponding deep level is (E_a=0.37 eV, $\sigma \sim 10^{-15}$ cm^2),[20,21] where E_a and σ are the activation energy an the apparent cross section, respectively.[10] After a filling pulse performed at temperature T, a concentration $n_{t0}=n_t(0,T)$ of these levels is filled with holes. The time $t=0$ is set at the end of the filling pulse: at this time a reverse bias is applied on the diode and the emission from this trap can be monitored. The time variation of the space charge density at the temperature T is given by

$$Q(t,T) = \pm qN_{\text{eff}}(t,T) = -qN_0(T) + qn_t(t,T). \tag{1}$$

The term $-q\cdot N_0(T)$ includes the contributions to the space charge density of the doping impurities and of all the energy levels which can be considered as frozen and filled at the temperature T. In this example it is assumed to be negative, but similar results are obtained with an electron trap and a positive $qN_0(T)$. In this case Eq. (1) would read: $Q=q\cdot N_0 - q\cdot n_t$. The current $i(t,T)$ emitted by the deep levels inside the depleted region is due to the holes released by C_iO_i. Thus Q becomes less and less positive as the defect discharges. Neglecting carrier recapture, the function $n_t(t,T)$ is given by[22]

$$\frac{dn_t(t,T)}{dt} = -e_h(T)\cdot n_t(t,T), \tag{2}$$

where $e_h(T)$ is the hole emission coefficient:

$$e_h(T) = \gamma_h \sigma T^2 \exp(-E_a/kT). \tag{3}$$

Here k is the Boltzmann constant and γ_h accounts for the band structure of the material. The current transient can be then calculated as

$$i(t,T) = \frac{q\cdot Z(t,T)}{2}\cdot e_h(T)\cdot n_t(t,T), \tag{4}$$

with Z being the volume of the depleted region. The dielectric relaxation time $t=\varepsilon\cdot\rho$ (ε is the absolute dielectric constant and ρ is the electrical resistivity) is always much smaller than the time scale ($\sim$1 ms) used in our transient measurements, and carriers can easily rearrange across the depleted region as the deep levels discharge. As a consequence, a quasistationary situation will be assumed in which, at any time t_0, the depleted region has the same volume it would have in stationary conditions, if the constant space charge density were $Q(t_0)$. The depleted region spreads inside the bulk following the electric field lines, and its shape can be determined by numerical simulations.[23] The results of simulations suggest that the volume Z of the depleted region can be roughly determined as shown in Fig. 2 (two different situations are shown in the figure, depending on whether the space charge density is inverted or not). Here, the depletion depth x_d is approximated using the expression valid for an abrupt planar junction:[24]

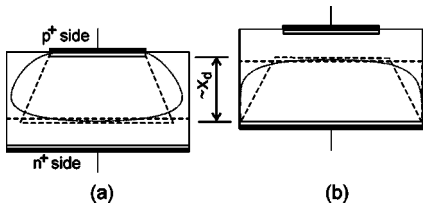

FIG. 2. Cross section of a diode showing the qualitative determination of the depleted region profile used in the text to estimate the depleted volume. The dotted lines indicate the geometric shape of the depleted region. The two regions used to estimate Z, a truncated pyramid and a squared box, are plotted by dashed lines. Black and gray areas indicate metallizations and implants, respectively. Scheme (a) refers to a noninverted bulk, while scheme (b) describe an inverted one. In the latter case the junction is shifted to the n^+ side.

$$x_d(t,T) = \sqrt{\frac{2\varepsilon V_{\text{rev}}}{qN_{\text{eff}}(t,T)}}. \tag{5}$$

The actual depleted region is smaller than a square box with depth x_d and base area A_n. On the other hand, it is larger than the volume of the truncated pyramid indicated in the figure. As a reasonable and simple evaluation of Z, we will use the average between the square box and the volume of the truncated pyramid.

In the limit $N_t \ll N_{\text{eff}}$, the depleted volume can be considered time independent, and the current transient retains the standard exponential form:

$$i(t,T) = \frac{qZn_{t0}e_h}{2}\exp(-e_h t). \tag{6}$$

The case of $N_t \approx N_{\text{eff}}$ shows different dynamics and is shown in Fig. 3 for a particular choice of n_{t0} and N_0($n_{t0}=5\times10^{12}$ cm^{-3}, $N_0=2.5\times10^{12}$ cm^{-3}). Several $N_{\text{eff}}(t,T)$ profiles calculated at different temperatures are shown in Fig. 3(c). At the lowest temperature (198 K) the trap discharge is quite slow, and $Q(t,T)$ becomes negative only at the end of the time interval of the figure. As T rises, the SCSI$^{+/-}$ takes place faster. In general the space charge density may change from positive to negative or vice versa, and these phenomena are indicated by SCSI$^{+/-}$ and SCSI$^{-/+}$, respectively. The active volume (normalized to the volume at full depletion) from which the collected current is emitted is shown in Fig. 3(b). As long as N_{eff} is smaller than a certain value N_{fd} the sample is fully depleted and the active volume reaches its maximal value. From Eq. (5) we obtain

$$N_{\text{fd}} = \frac{2\varepsilon V_{\text{rev}}}{qw^2}, \tag{7}$$

w being sample thickness. The calculated current transients are shown in Fig. 3(a). Three characteristic stages in the $i(t,T)$ evolution can be distinguished, as indicated in the figure. The current rises as the depleted volume increases. A pronounced current spike occurs when $N_{\text{eff}} \sim 0$ (during full depletion and SCSI). After this SCSI the absolute value of N_{eff} continues to grow and leads to a decrease of the depletion width. In consequence the current decreases as well. At

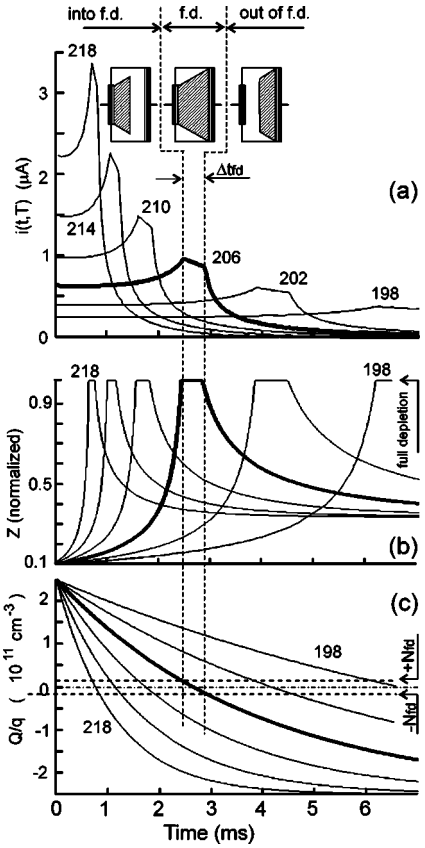

FIG. 3. Calculated dynamics of current emission from a hole trap dominating the space charge density. Current transients (a), active volume Z (b), and space charge density $Q(t,T)$ calculated at different temperatures (c) are shown. The curves corresponding to the temperature $T=206$ K are plotted with a thicker lines to guide the eye. The space charge density has been normalized to elementary charge q. For $T=206$ K, a schematic illustration of the diode cross section, indicating the depleted volume, is shown at the top of the figure. The shaded and the black areas are the depleted regions and the metallizations, respectively.

the end of this last stage, the depleted volume tends to its steady state under the applied reverse bias and the transients approach an exponential behavior.

IV. EXPERIMENTAL RESULTS AND DISCUSSION

A. Current transient analysis

The discussion will focus on the charge emissions from two deep levels observed both in irradiated STFZ and DOFZ silicon. The first level is related to the already mentioned "interstitial carbon-interstitial oxygen" complex $C_iO_i^{+/0}$, and the second to the single charged state of double vacancy $V_2^{-/0}$ ($E_a=0.42$ eV, $\sigma\cong 2\times 10^{-15}$ cm^2).[21,25] The introduction of these levels in silicon after γ irradiation has been widely investigated, starting from the work of Brotherton and Bradley[26] (see, e.g., Moll *et al.*[27] for a general overview). The concentration of such defects in our samples is of the order of 10^{13} cm^{-3}, as it can be deduced from the amplitude of TSC spectra shown in the next section. Note that C_iO_i and V_2 are not responsible for the different value of N_{eff} at room

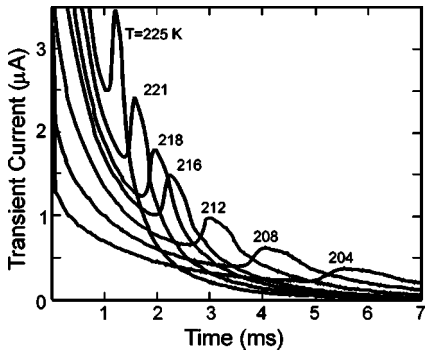

FIG. 4. Current transients measured in the DOFZ sample in the range 204–225 K. $V_{\text{rev}}=10$ V, $V_p=7$ V, $t_p=100$ μs. A step in the current transient occurs at a time which is reduced as temperature grows. The numbers typed above each transient indicate the temperature at which the measurement was performed.

temperature in irradiated STFZ and DOFZ Si devices. This is because at room temperature these levels are almost completely uncharged. The different value of N_{eff} measured at room temperature is due mainly to the presence in γ-irradiated STFZ Si of a deeper defect, the so-called "I defect," characterized by an acceptor level with $E_a=0.54$ eV, whose concentration is strongly reduced in DOFZ Si.[28,29]

The evolution of current transients at constant temperature in the DOFZ sample, in the range 204–225 K, is shown in Fig. 4. In this temperature range the current transient is due mainly to the C_iO_i discharge. At each temperature, an abrupt irregularity (a nonmonotonic feature resembling a "peak" in the current profile) is observed.

The resemblance of these measurements with the simulations of Fig. 3 is striking. As a matter of fact, the main features of the measured transients can be accounted for in terms of SCSI$^{+/-}$ by using Eqs. (1)–(6). As an example, a fit to the signal measured at 216 K is shown in Fig. 5. The measured current transient (for an applied voltage of 10 V) and the calculated one are shown in Fig. 5(c). There is a good agreement between them, even if the details of the experimental result cannot be fully reproduced by our simple model. In particular, the behavior before and after SCSI, as well as the position of the full depletion peak and its width can be very well described. The time evolution of depleted volume $Z(t)$ and of $N_{\text{eff}}(t)$ are shown in Figs. 5(a) and 5(b), respectively. The initial values used for the simulation are $N_t(0,216\text{ K})=2.0\times 10^{13}$ cm^{-3} for C_iO_i concentration and $-qN_0=-q\cdot 1.2\times 10^{13}$ cm^{-3} for background space charge density. $Q(t)$ starts from the positive value $Q(0)=q(N_t-N_0)$, ending to the negative value $-qN_{\text{eff}}(\infty)=-qN_0$. The SCSI$^{+/-}$ takes place at about $t=2.5$ ms. Around this point, as long as $N_{\text{eff}}<N_{\text{fd}}$, the sample is fully depleted. The width of the peak corresponds to the time spent at full depletion and, according to Eq. (7), is proportional to the applied bias. Two main features of the current peaks shown in Fig. 4 are

(1) the peak occurs earlier as T increases (for instance, at $T=204$ K the peak is observed beyond $t=5$ ms, while at $T=225$ K the peak is close to $t=1.2$ ms).

(2) The rising edge of the peak becomes steeper and steeper as the temperature increases.

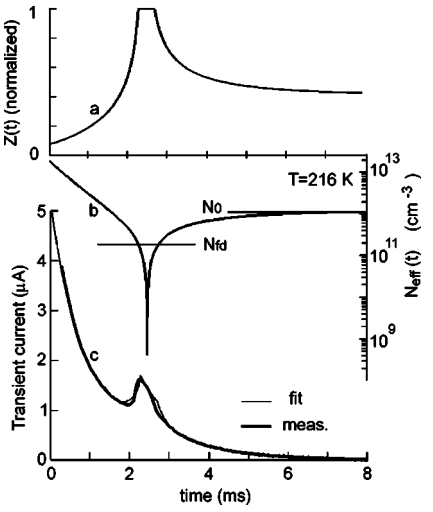

FIG. 5. A fit of current transient measured in DOFZ Si at $T=216$ K obtained with Eqs. (1)–(5). The applied reverse bias during measurement is $V_{rev}=10$ V. Calculated evolution with time of N_{eff} (b) and of depleted volume Z (a) are shown above the current transient (c). The depleted volume is normalized to the value at full depletion. The steady state effective doping concentration N_0 reached after a complete C_iO_i discharge and the highest N_{eff} value which permits full depletion (N_{fd}) are shown.

These two facts (which are common to all the transients shown in the following) are consistent with the proposed picture: the higher the temperature, the faster the trap discharge and the occurrence of type inversion.

Nonmonotonic current transients are not unique to γ irradiated DOFZ silicon. Current transients similar to those of Fig. 4 have been observed also in the STFZ sample, as shown in Fig. 6. The current peaks can be explained in terms of SCSI occurring during hole emission from C_iO_i in this case, as well.

Additional measurements aimed at studying the dependence of transient shape on the value of the reverse bias have been carried out. The results obtained with the oxygenated sample at $T=231$ K are shown in Fig. 7. Note that these measurements have been carried out six months after the experiments reported in Fig. 4. During this time the sample was stored at room temperature, and a modification of deep level population occurred, determining a different ratio between the concentrations of positively and negatively charged traps. Now, for the different applied bias voltages,

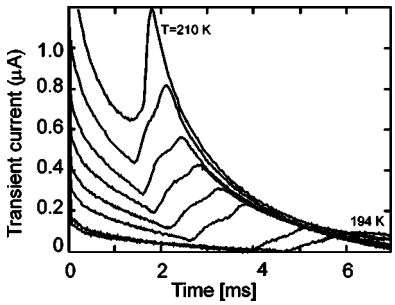

FIG. 6. Current transients in the STFZ sample, corresponding to different temperatures in the range from 194 K (weaker signal) to 210 K (stronger signal). $V_{rev}=10$ V, $V_p=7$ V, and $t_p=100$ μs.

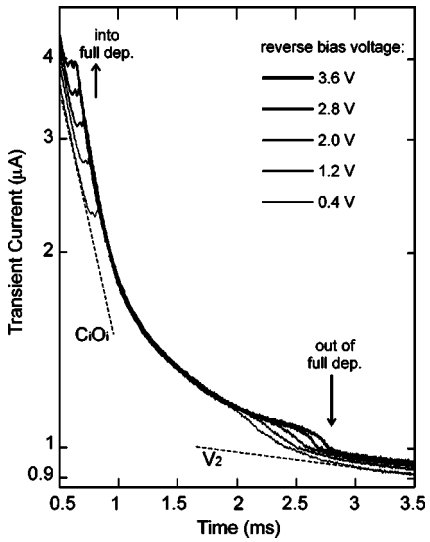

FIG. 7. Current transient measured at $T=231$ K in DOFZ sample (after 6 additional months storing at room temperature) using various reverse biases, as indicated in the legend. The vertical axis is plotted using a logarithmic scale. Two straight lines whose slope corresponding to C_iO_i and V_2 emissions are indicated too. The arrows indicate the time at which the sample becomes fully depleted (near 1 ms), and the time at which the formerly depleted sample becomes partially depleted again (near 2.5 ms). $V_p=7$ V, $t_p=100$ μs.

the current transients exhibit two discontinuities. The first one occurs when, during the C_iO_i discharge, the samples enter into full depletion. The time at which this transition appears depends on the bias voltage and is shifted to shorter times for increasing bias voltage. After this period all recorded transient values are independent of the reverse bias up to a certain time where the second discontinuity occurs. During the time interval between the two discontinuities the device remains fully depleted for each applied bias and the active volume is fixed by the geometry of the sample. The second discontinuity occurs as the space charge density becomes larger and positive after some electron emission from V_2. Thus for a given bias voltage the device cannot remain fully depleted, and this leads to an abrupt decrease of the current signal. Before and after the discontinuities the activation energies of C_iO_i and V_2 determine the slope of the current transient, as shown by the dotted lines in the figure, and the signal intensity rises as long as the bias voltage is increased.

B. TSC analysis on DOFZ silicon

One question to be answered is if TSC measurements are in agreement with transient analysis in predicting that C_iO_i and V_2 dominate the space charge density when they start discharging. The TSC spectrum measured with $V_{rev}=10$ V is shown in Fig. 8 as a thick solid line connecting experimental points, while the fit components are plotted with thin solid lines. Two main emissions are found in the range 100–200 K. The first is the hole emission from $C_iO_i^{+/0}$ and the other is the electron emission from $V_2^{-/0}$. Below 137 K, the signal can be fitted by a deep level with activation energy

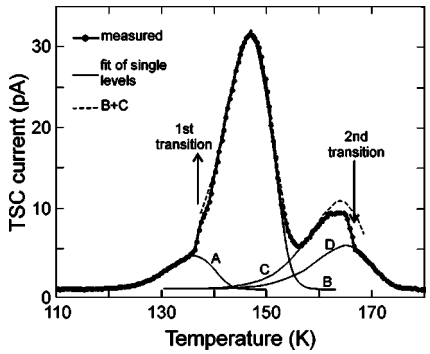

FIG. 8. TSC spectrum of the DOFZ sample measured in the range 110–180 K with $V_{rev}=10$ V. The heating rate is 0.1 K/s. Thin solid lines (A–C) correspond to the calculated contribution of discrete deep levels. The dashed line corresponds to the sum B+C, while the thick solid line connecting the experimental points is the measured current.

close to 0.3 eV (line A). Then, as soon as C_iO_i starts to emit, a discontinuity (indicated as "1st transition" in the figure) occurs, and the current jumps toward higher value. This transition is similar to the jump reported in Ref. 8 near 150 K, caused by a $SCSI^{+/-}$ leading to an increase of the active volume. After this transition, the signal can be well fitted by the $C_iO_i^{+/0}$ contribution (line B) plus the $V_2^{-/0}$ contribution (line C). The sum of these two components (B+C) is shown as a dashed line. Above 160 K the signal undergoes a second abrupt transition toward lower current values. This second transition corresponds to a $SCSI^{-/+}$ which reduces again the depleted volume. After the second transition the signal profile can be well fitted by an attenuated V_2 contribution (line D).

The TSC measurements were repeated using a higher reverse voltage, $V_{rev}=100$ V, which ensures an almost full depletion of the sample over the full TSC temperature range. The result is shown in Fig. 9. Now the spectrum is smoothened and can be completely fitted by $C_iO_i^{+/0}$ and $V_2^{-/0}$ contributions. This is because in this case the bulk is permanently fully depleted during the measurement and the total active volume uniquely determined by the geometry of the sample, independently of traps charge state and N_{eff} value.

Using $V_{rev}=100$ V the signal-to-noise ratio is improved, and a peak near 207 K can be distinguished. It corresponds

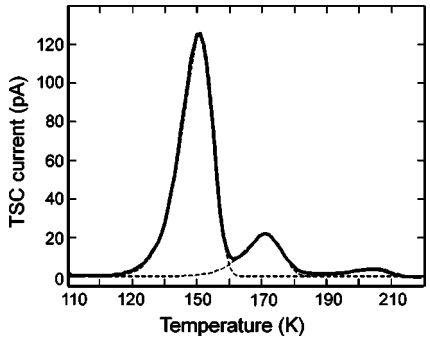

FIG. 9. TSC spectrum of the DOFZ sample measured in the range 110–220 K with $V_{rev}=100$ V, heating rate 0.15 K/s. Dashed lines correspond to the calculated contribution of $C_iO_i^{+/0}$ (peak at 150 K) and $V_2^{-/0}$ (peak close to 170 K).

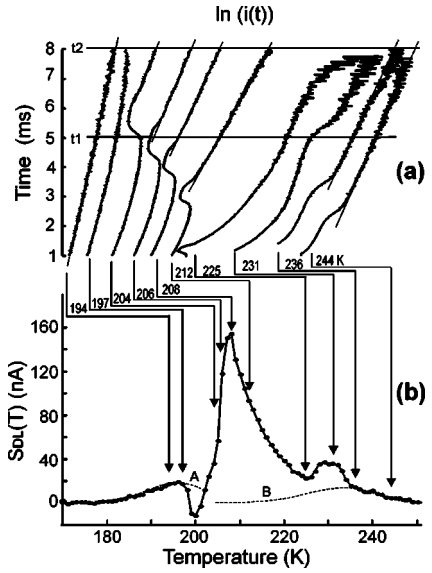

FIG. 10. Current transients at constant temperature (a) and DLTS spectrum (b) of the DOFZ sample. The current transients are plotted on a logarithmic scale. The sampling times used to calculate the DLTS spectrum ($t_1=5$ ms, $t_2=8$ ms), are indicated in the upper plot by horizontal lines. The dotted lines A and B correspond to the contributions calculated for $C_iO_i^{+/0}$ and $V_2^{-/0}$, respectively. A vertical arrow connects each transient to the corresponding point in the spectrum; the transient temperature is indicated near the arrow (and corresponds to the abscissa on the temperature axis). $V_{rev}=10$ V, $V_p=7$ V.

to the emission from the acceptor level close to midgap related to the "I defect."

C. Effect on DLTS spectra

Usually the current transients are analyzed to determine the current-DLTS spectrum. A common procedure is to define the spectrum $S_{DL}(T)$ as

$$S_{DL}(T) = i(t_1,T) - i(t_2,T). \tag{8}$$

Here t_1 and t_2 are the transient sampling times. If the transients are exponential, $S_{DL}(T)$ can be analyzed (e.g., by numerical fitting or by an Arrhenius plot) in order to find out deep level signatures and concentrations. However, if the transients are similar to those shown in Sec. IV A, this procedure cannot be followed. Nevertheless, it is interesting to analyze the peculiar effect of nonmonotonic transients on a DLTS spectrum, due to the wide use of this technique. Here we show how a distortion in the DLTS spectrum can be related to carrier emission from a trap strongly influencing $N_{eff}(T)$.

The relationship between the nonmonotonic current transients $i(t,T)$ flowing through the sample and the shape of the spectrum $S_{DL}(T)$ is shown in Fig. 10. The logarithm of a few selected current transients measured at different temperatures are displayed in Fig. 10(a). The curves are placed one beside the other to obtain a clear plot, and their absolute positions do not provide information (see Fig. 4 for a comparison of their relative amplitude). In this graph a purely exponential

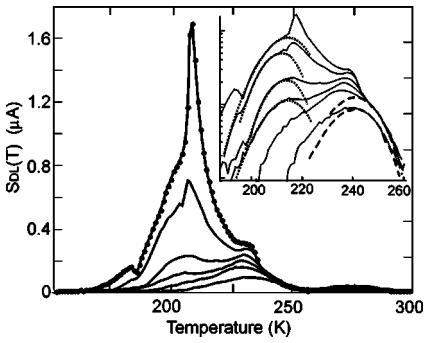

FIG. 11. I-DLTS spectra measured on DOFZ using different filling (forward) voltages V_P. These voltages are, moving from the weaker to the stronger signal, $V_p=0.5$, 0.7, 1, 1.2, 1.5, and 7 V. The other experimental parameters are $V_{\mathrm{rev}}=10$ V, $t_p=100$ μs, $t_1=1$ ms, and $t_2=8$ ms. The same signals, plotted on a logarithmic scale, are shown in the inset (solid lines) superimposed to the fit of $C_iO_i^{+/0}$ (dotted lines) and $V_2^{-/0}$ (dashed lines).

transient is plotted as a straight line. The sampling times t_1 and t_2 are indicated too. The corresponding DLTS spectrum is shown in Fig. 10(b). An arrow guides the eye from every transient to the corresponding spectrum point. Below 195 K the transients are exponential and the spectrum can be fitted to Eq. (7) using the C_iO_i signature (dotted line A). Above 195 K a peak in the current transient associated with a $SCSI^{+/-}$ appears. It moves toward shorter times as T increases, leading to a distortion of the DLTS spectrum. Thus when the $SCSI^{+/-}$ occurs between t_1 and t_2, $i(t_2,T)$ abruptly grows while $i(t_1,T)$ remains almost constant. The result is a negative $S_{\mathrm{DL}}(T)$. At $T=204$ K the peak in the current transient crosses the time t_1. At this point $i(t_1,T)$ grows too: S_{DL} exhibits a strong increase and becomes positive again. Note that, as long as the C_iO_i emission is dominant (up to 212 K in the figure) and far from the peak, the transient can be fitted by the exponential C_iO_i contribution. Despite this, the spectrum S_{DL} cannot be fitted, since the transient is not exponential in the whole time interval between t_1 and t_2. The transient fit is shown by straight thin lines in Fig. 10(a). Between 225 and 231 K, $i(t_2,T)$ decreases and the S_{DL} signal grows. This is because, above 225 K, the electron emission from V_2 starts changing N_{eff} toward a positive value. As discussed in Sec. IV A, the decreasing step observed in the current transients during the discharge of V_2 can be explained considering a $SCSI^{-/+}$ when, during the transient, the active volume of the sample changes dramatically.

At about 230 K the decreasing step crosses t_1. Above this temperature Q remains positive during the whole interval (t_1,t_2) and the exponential shape of the $V_2^{-/0}$ emission starts to be recovered. The result is that both the transients and the spectrum can be fitted by means of the $V_2^{-/0}$ signature (dotted line B).

The DLTS spectra measured using different forward excitation voltages V_{p}, in the range $V_{\mathrm{p}}=0.1-7$ V, are shown in Fig. 11. Here the sampling times are different with respect to those used in Fig. 10. Comparing Figs. 10 and 11, we note that the peak of the signal does not move to lower temperatures by increasing the time window as for standard DLTS: this is because the signal is heavily distorted. The signal from C_iO_i, which is a minority carrier trap, is significant only if a sufficient forward injection takes place, while the $V_2^{-/0}$ contribution is always observed. The discontinuities near 230 K, which are related to V_2 (a majority carrier trap) can be seen as soon as $V_{\mathrm{p}}\geqslant 1$ V. On the contrary, the discontinuity near 190 K, related to C_iO_i (which is a minority carrier trap) can be seen only if a stronger forward bias is applied during excitation. In the inset, the curves of the main graph have been plotted on a logarithmic scale (solid lines). The calculated contribution of $C_iO_i^{+/0}$ (dotted lines) and $V_2^{-/0}$ (dashed lines) are shown as well. As expected, before and after the discontinuities at 220 and 240 K, the spectra can be fitted by standard contributions.

Distorted current DLTS spectra have been already measured in the past on high resistivity irradiated silicon[30] and on semi-insulating GaAs.[31] In the latter work it was suggested that the distortion, and in particular the negative side of the DLTS peak, should be related to SCSI, but no quantitative description of the phenomenon was given.

V. CONCLUSIONS

Nonmonotonic current transients at constant temperature, following a pulsed carrier injection, have been observed in standard float zone and diffusion oxygenated float zone silicon diodes irradiated with a high total dose (300 Mrad) of gamma rays from a Co^{60} source. The features of the transients are studied at different temperatures and they are correlated to irregularities observed in TSC measurements.

The particular shape of the current transients is interpreted in terms of strong space charge density modifications due to the discharge of the dominating traps (double vacancy and oxygen-carbon complex in the explored temperature range) producing a change in the space charge sign (type inversion or space charge sign inversion). Our experimental and simulation work shows that the study of current transient is a sensitive tool to determine the occurrence of type inversion in semiconductor devices and quite effective in relating this phenomenon to the responsible energy levels.

The effect of nonmonotonic transients on DLTS spectra is discussed. The resulting spectra are strongly distorted and do not allow performing a standard analysis of the deep level signatures. However, our analysis of the current transients provides a powerful tool for the correct interpretation of these measurements. Current transient analysis appears therefore an accurate technique in detecting space charge modifications and type inversion during the emission of nonequilibrium carriers from dominating defects, produced in our case by high doses of γ irradiation.

ACKNOWLEDGMENTS

This work has been performed in the framework of the CERN RD50 collaboration and financially supported by the INFN project SMART. We wish to thank Andrea Baldi from University of Florence for technical support to this work. We warmly thank Z. Li from BNL, E. Verbitskaya, and V. Eremin from IOFFE, St. Petersburg, and H. F. W. Sadrozinski from Santa Cruz Institute for Particle Physics for helpful discussions.

*Author to whom correspondence should be addressed. Electronic address: menichelli@ingfi1.ing.unifi.it

[1] M. Jaros, *Deep Levels in Semiconductors* (Adam Hilger, Bristol, 1982).
[2] M. Bruzzi, IEEE Trans. Nucl. Sci. **48**, 960 (2000).
[3] G. Lindstroem, Nucl. Instrum. Methods Phys. Res. A **512**, 30 (2003).
[4] D. Creanza, M. De Palma, V. Radicci, L. Schiavulli, K. I. Hinz, G. W. Rossberg, J. Kierstead, Z. Li, A. Cavallini, S. Lazanu, *et al.*, RD50 Status Report 2002/2003, CERN-LHCC-2003-058, 2003.
[5] R. Wunstorf, Nucl. Instrum. Methods Phys. Res. A **466**, 327 (2001).
[6] Z. Li, C. J. Li, and E. Verbitskaya, IEEE Trans. Nucl. Sci. **44**, 834 (1997).
[7] E. Fretwurst, V. Eremin, H. Feick, J. Gerhardt, Z. Li, and G. Lindström, Nucl. Instrum. Methods Phys. Res. A **338**, 356 (1997); E. Verbitskaya,M. Abreu, P. Anbinderis, T. Anbinderis, N. D'Ambrosio, W. de Boer, E. Borchi, K. Borer, M. Bruzzi, S. Buontempo, *et al.*, *ibid.* **514**, 47 (2003).
[8] I. Pintilie, L. Pintilie, M. Moll, E. Fretwurst, and G. Lindstroem, Appl. Phys. Lett. **78**, 550 (2001).
[9] M. G. Buhler, Solid-State Electron. **15**, 69 (1972).
[10] P. Blood and J. W. Orton, *The Electrical Characterization of Semiconductors: Majority Carriers and Electron States* (Academic, London, 1992).
[11] D. V. Lang, J. Appl. Phys. **45**, 3023 (1974).
[12] B. W. Wessels, J. Appl. Phys. **47**, 1131 (1976).
[13] C. H. Hurtes, M. Boulou, A. Mitonneau, and D. Bois, Appl. Phys. Lett. **32**, 821 (1978).
[14] A. C. Wang and C. T. Sah, J. Appl. Phys. **55**, 565 (1984).
[15] W. E. Phillips and J. R. Lowney, J. Appl. Phys. **54**, 2786 (1983).
[16] E. Rosencher, V. Mosser, and G. Vincent, Phys. Rev. B **29**, 1135 (1984).
[17] Z. Li, H. W. Kraner, E. Verbitskaya, V. Eremin, A. Ivanov, M. Rattaggi, P. G. Rancoita, F. A. Rubinelli, S. J. Fonash, C. Dale, and P. Marshall, IEEE Trans. Nucl. Sci. **39**, 1730 (1992).
[18] G. Lindström, M. Ahmed, S. Albergo, P. Allport, D. Anderson, L. Andricek, M. M. Angarano, V. Augelli, N. Bacchetta, P. Bartalini, *et al.*, Nucl. Instrum. Methods Phys. Res. A **465**, 60 (2001).
[19] J. M. Trombetta and G. D. Watkins, Appl. Phys. Lett. **57**, 1103 (1987).
[20] M. Mamor, M. Willander, F. D. Auret, W. E. Meyer, and E. Sveinbjörnsson, Phys. Rev. B **63**, 045201 (2001); A. Khan, M. Yamaguchi, T. Hisamatsu, and S. Matsuda, J. Appl. Phys. **87**, 2162 (2000).
[21] A. Hallén, N. Keskitalo, F. Masszi, and V. Nágl, J. Appl. Phys. **79**, 3906 (1996).
[22] W. Shockley and W. T. Read, Jr., Phys. Rev. **87**, 835 (1952).
[23] R. Sonnenblick, N. Cartiglia, B. Hubbard, J. Leslie, H. F. W. Sadrozinski, and T. Schalk, Nucl. Instrum. Methods Phys. Res. A **310**, 189 (1991); D. Husson, IEEE Trans. Nucl. Sci. **41**, 811 (1994); Z. Li, D. Anderson, B. Barnett, R. Beuttenmueller, W. Chen, C. Y. Chien, V. Eremin, M. Frautschi, G. Grim, G. Hu, S. Kwan, D. Lander, S. Mani, S. U. Pandey, Q. Wang, S. Willard, and X. Xie, Nucl. Instrum. Methods Phys. Res. A **409**, 180 (1998).
[24] S. M. Sze, *Physics of Semiconductor Devices* (Wiley, New York, 1981).
[25] G. D. Watkins and J. W. Corbett, Phys. Rev. **138**, A543 (1965).
[26] S. D. Brotherton and P. Bradley, J. Appl. Phys. **53**, 5720 (1982).
[27] M. Moll, H. Feick, E. Fretwurst, G. Lindström, and C. Schütze, Nucl. Instrum. Methods Phys. Res. A **388**, 335 (1997).
[28] I. Pintilie, E. Fretwurst, G. Lindstroem, and J. Stahl, Appl. Phys. Lett. **82**, 2169 (2003).
[29] I. Pintilie, E. Fretwurst, G. Lindström, and J. Stahl, Nucl. Instrum. Methods Phys. Res. A **514**, 18 (2003).
[30] Z. Li, C. J. Li, and E. Verbitskaya, IEEE Trans. Nucl. Sci. **44**, 834 (1997), see Fig. 6.
[31] E. Verbitskaya, V. Eremin, A. Ivanov, N. Strokan, V. Vasilev, A. Markov, A. Polyakov, V. Gravin, Y. Kozlova, E. Veretenkin, and T. J. Bowles, Nucl. Instrum. Methods Phys. Res. A **439**, 634 (2000), see p. 644 and Fig. 4.